

Adjustable half-skyrmion chains induced by SU(3) spin-orbit coupling in rotating Bose-Einstein condensates

Li Wang(王力), Ji Li(李吉), Xiao-Lin Zhou(周晓林), Xiang-Rong Chen(陈向荣), and Wu-Ming Liu(刘伍明)
Citation: Chin. Phys. B, 2021, 30 (**11**): 110312. DOI: 10.1088/1674-1056/abfcc8
Journal homepage: http://cpb.iphy.ac.cn; http://iopscience.iop.org/cpb

What follows is a list of articles you may be interested in

Spin-orbit-coupled spin-1 Bose-Einstein condensates confined in radially periodic potential

Ji Li(李吉), Tianchen He(何天琛), Jing Bai(白晶), Bin Liu(刘斌), and Huan-Yu Wang(王寰宇)
Chin. Phys. B, 2021, 30 (**3**): 030302. DOI: 10.1088/1674-1056/abc53e

Lattice configurations in spin-1 Bose–Einstein condensates with the SU(3) spin–orbit coupling

Ji-Guo Wang(王继国)†, Yue-Qing Li(李月晴), and Yu-Fei Dong(董雨菲)
Chin. Phys. B, 2020, 29 (**10**): 100304. DOI: 10.1088/1674-1056/abab72

Interference properties of two-component matter wave solitons

Yan-Hong Qin(秦艳红), Yong Wu(伍勇), Li-Chen Zhao(赵立臣), Zhan-Ying Yang(杨战营)
Chin. Phys. B, 2020, 29 (**2**): 020303. DOI: 10.1088/1674-1056/ab65b7

Periodically modulated interaction effect on transport of Bose-Einstein condensates in lattice with local defects

Kun-Qiang Zhu(朱坤强), Zi-Fa Yu(鱼自发), Ji-Ming Gao(高吉明), Ai-Xia Zhang(张爱霞), Hong-Ping Xu(徐红萍), Ju-Kui Xue(薛具奎)
Chin. Phys. B, 2019, 28 (**1**): 010307. DOI: 10.1088/1674-1056/28/1/010307

Trapped Bose-Einstein condensates with quadrupole-quadrupole interactions

An-Bang Wang(王安邦), Su Yi(易俗)
Chin. Phys. B, 2018, 27 (**12**): 120307. DOI: 10.1088/1674-1056/27/12/120307

Adjustable half-skyrmion chains induced by SU(3) spin–orbit coupling in rotating Bose–Einstein condensates*

Li Wang(王力)[1], Ji Li(李吉)[2,†], Xiao-Lin Zhou(周晓林)[3], Xiang-Rong Chen(陈向荣)[1], and Wu-Ming Liu(刘伍明)[4,5,6,‡]

[1] *College of Physics, Sichuan University, Chengdu* 610065, *China*
[2] *College of Physics, Taiyuan Normal University, Jinzhong* 030619, *China*
[3] *School of Physics and Electronic Engineering, Sichuan Normal University, Chengdu* 610101, *China*
[4] *Beijing National Laboratory for Condensed Matter Physics, Institute of Physics, Chinese Academy of Sciences, Beijing* 100190, *China*
[5] *School of Physical Sciences, University of Chinese Academy of Sciences, Beijing* 100190, *China*
[6] *Songshan Lake Materials Laboratory, Dongguan* 523808, *China*

(Received 24 March 2021; revised manuscript received 28 April 2021; accepted manuscript online 29 April 2021)

The ground state properties of the rotating Bose–Einstein condensates (BECs) with SU(3) spin–orbit coupling (SOC) in a two-dimensional harmonic trap are studied. The results show that the ferromagnetic and antiferromagnetic systems present three half-skyrmion chains at an angle of 120° to each other along the coupling directions. With the enhancement of isotropic SU(3) SOC strength, the position of the three chains remains unchanged, in which the number of half-skyrmions increases gradually. With the increase of rotation frequency and atomic density–density interaction, the number of half-skyrmions on the three chains and in the regions between two chains increases gradually. The relationships of the total number of half-skyrmions on the three chains with the increase of SU(3) SOC strength, rotation frequency and atomic density–density interaction are also given. In addition, changing the anisotropic SU(3) SOC strength can regulate the number and morphology of the half-skyrmion chains.

Keywords: Bose–Einstein condensates, SU(3) spin–orbit coupling, rotation, half-skyrmion chains

PACS: 03.75.Lm, 03.75.Hh, 03.75.Nt, 05.30.Jp **DOI:** 10.1088/1674-1056/abfcc8

1. Introduction

The realization of spinor Bose–Einstein condensates (BECs) in an optical dipole trap provides an ideal experimental platform to study many fantastic topological defects, such as spin vortex, vortex lattice, skyrmion, monopole and knot.[1–10] Especially in recent years, the realization of artificial spin–orbit coupling (SOC) in cold atomic gases has made SOC spinor BECs become a hot research topic in the field of cold atomic physics, providing a new opportunity to explore novel quantum phenomena and topological quantum states, such as topological insulators, quantum spin Hall effect and topological superconductors.[11–25]

The SOC effect mainly describes the coupling between the orbital motion of a particle and its spin.[26] Experimentally, the one-dimensional (1D) and two-dimensional (2D) SOC have been realized in ultracold atoms,[14,24,27,28] and researchers have also proposed different realization schemes in theory.[15–17,23,29–33] The common forms of SOC are Rashba-type, Dresselhaus-type and Rashba–Dresselhaus-type.[14,34,35] In previous work, people focused on SU(2) SOC, namely, the coupling between the spin operator and the momentum operator represented via the SU(2) Pauli matrices. However, if there are more than two states in the spin degree of freedom, the SU(2) spin matrices cannot fully describe the coupling of all the internal states. For example, in a three-component system, the direct transition between the states $|1\rangle$ and $|-1\rangle$ will be ignored.[21] At this moment, the SU(3) SOC with the spin operator spanned by the Gall–Mann matrices can more completely describe the internal couplings among the three-component atoms.[36] In addition, the BECs with SU(3) SOC will produce a new topological defect, i.e., the double-quantum spin vortex.[37] Depending on the spin-exchange interaction, there are two different ground state phases. The ferromagnetic spin-exchange interaction produces the magnetized phase, and the antiferromagnetic spin-exchange interaction produces the lattice phase. In the magnetized phase, SU(3) SOC leads to a ground state with threefold degeneracy, in stark contrast to the SU(2) case where the degeneracy is twofold.[21] In the lattice phase, the SU(3) SOC breaks the phase conditions for ordinary spinor BECs, resulting in three novel vortices with different magnetized cores.[36,38]

Recently, Li *et al*. studied the effect of spin-dependent

*Project supported by the National Key Research and Development Program of China (Grant No. 2016YFA0301500), the National Natural Science Foundation of China (Grant Nos. 61835013 and 11971067), the Strategic Priority Research Program of the Chinese Academy of Sciences (Grant Nos. XDB01020300 and XDB21030300), the Beijing Natural Science Foundation, China (Grant No. 1182009), and the Beijing Great Wall Talents Cultivation Program (Grant No. CIT&TCD20180325).

†Corresponding author. E-mail: liji163love@163.com
‡Corresponding author. E-mail: wmliu@iphy.ac.cn

© 2021 Chinese Physical Society and IOP Publishing Ltd

interaction and SU(3) SOC on the BECs in a harmonic plus quartic trap. The results showed that SU(3) SOC can generate a threefold-degenerate plane wave phase with nontrivial spin texture for ferromagnetic spin interaction case. However, for antiferromagnetic spin interaction case, the strong SU(3) SOC could produce the hexagonal honeycomb lattice structure.[39] Yue *et al*. studied the ground state and metastable solution of solitons in BECs with SU(3) SOC by the imaginary-time evolution method.[40] Wang *et al*. studied the ground state of BECs with isotropic and anisotropic SU(3) SOC in a 2D harmonic trap. It was found that the competition between the SU(3) SOC and the spin-exchange interaction produces abundant lattice phases, such as the kagome lattice phase, the stripe-honeycomb lattice phase and the honeycomb hexagonal lattice phase.[41] Considering the rotation effect, the ground state of the BECs with SU(2) SOC had been extensively studied, such as the triangular vortex lattice with giant skyrmion in the center, the ring-hyperbolic skyrmion, and the half-skyrmion chain along the diagonal.[42–51] However, the research on the ground state of SU(3) SOC rotating BECs system is relatively rare. Peng *et al*. studied the ground state of BECs with SU(3) SOC in a harmonic trap, and numerically calculated the 2D density, phase and magnetization distribution of the ground state under different parameters. They found that a new ground state with a clover-type structure in the density distribution of the condensate is induced by rotation. Once the rotation frequency increased and exceeded a critical value, the vortex with one or several cores appeared in the three parts of the structure.[52]

In this paper, the ground state properties of the rotating BECs with isotropic and anisotropic SU(3) SOC in a 2D harmonic trap are further investigated. By numerically solving the Gross–Pitaeviskii equations of the mean field approximation, the effects of the external parameters on the ground state of BECs are discussed in detail. The results show that the ferromagnetic and antiferromagnetic systems present three half-skyrmion chains at an angle of 120° to each other along the coupling directions. With the enhancement of isotropic SU(3) SOC strength, the position of the three chains remains unchanged, in which the number of half-skyrmions increases gradually. With the increase of rotation frequency and atomic density–density interaction, the number of half-skyrmions on the three chains and in the regions between two chains increases gradually, and the surface area distribution of the condensate increases. However, different spin-dependent interactions have little effect on the ground state. Furthermore, the relationships of the total number of half-skyrmions on three chains with the increase of SU(3) SOC strength, rotation frequency and atomic density–density interaction are given. In addition, changing the anisotropic SU(3) SOC can regulate the number and morphology of half-skyrmion chains. Finally, the spin textures of the ground state under some specific parameters are discussed.

2. Model and Hamiltonian

We consider a three-component rotating BECs system with SU(3) SOC in a 2D harmonic trap. The Hamiltonian can be written as[51,52]

$$H=\int \mathrm{d}^2\boldsymbol{r}\Big\{\boldsymbol{\Psi}^{\dagger}\left(-\hbar^2\nabla^2/(2m)+V(\boldsymbol{r})+\nu_{\mathrm{soc}}+\Omega' L_z\right)\boldsymbol{\Psi} +\Big(\frac{c_0}{2}n^2+\frac{c_2}{2}\left[(n_1-n_{-1})^2+2|\Psi_1^*\Psi_0+\Psi_0^*\Psi_{-1}|^2\right]\Big)\Big\}, \quad (1)$$

where the order parameter $\boldsymbol{\Psi}=[\Psi_1(\boldsymbol{r}),\Psi_0(\boldsymbol{r}),\Psi_{-1}(\boldsymbol{r})]^{\mathrm{T}}$ can be normalized by the total number of particles $N=\int \mathrm{d}^2\boldsymbol{r}\boldsymbol{\Psi}^{\dagger}\boldsymbol{\Psi}$. The total particle density is $n=\sum_{m=1,0,-1}\Psi_m^*(\boldsymbol{r})\Psi_m(\boldsymbol{r})$. In the kinetic term, m is the mass of a ^{87}Rb atom and $\hbar$ is the Planck constant. The 2D harmonic potential can be expressed as $V(\boldsymbol{r})=\frac{1}{2}m[\omega^2(x^2+y^2)]$, wherein ω is the trapping frequency. The SU(3) SOC term is given by $\nu_{\mathrm{soc}}=\kappa_x\gamma_x p_x+\kappa_y\gamma_y p_y$, with κ_x and κ_y describe SU(3) SOC strengths in the x and y directions, respectively. $\kappa_x=\kappa_y=\kappa$ represents isotropic SU(3) SOC, and $\kappa_x\neq\kappa_y$ is for anisotropic SU(3) SOC. p_x and p_y represent the momentums in the x and y directions, respectively. γ_x and γ_y are expressed in terms of $\gamma_x=\gamma^{(1)}+\gamma^{(4)}+\gamma^{(6)}$ and $\gamma_y=\gamma^{(2)}-\gamma^{(5)}+\gamma^{(7)}$ through Gell–Mann matrices $\gamma^{(i)}$ $(i=1,\ldots,8)$.[53] Ω' is the rotation frequency, and $L_z=-\mathrm{i}\hbar(x\partial_y-y\partial_x)$ is the orbital angular-momentum along z direction. The coupling parameters of the interaction term are $c_0=4\pi\hbar^2(a_0+2a_2)/3m$ and $c_2=4\pi\hbar^2(a_2-a_0)/3m$, where $a_{0,2}$ are two-body s-wave scattering lengths for total spin $0,2$. The ground state and dynamic process of spin-1 BECs with SU(3) SOC can be described by the following quasi-2D dimensionless coupled nonlinear equations:

$$\begin{aligned}\mathrm{i}\frac{\partial\psi_1}{\partial t}=&\Big(-\frac{1}{2}\nabla^2+V+\mathrm{i}\Omega(x\partial_y-y\partial_x)+\lambda_0\rho\\&+\lambda_2(\rho_1+\rho_0-\rho_{-1})\Big)\psi_1+(-\mathrm{i}\kappa_x\partial_x-\kappa_y\partial_y)\psi_0\\&+(-\mathrm{i}\kappa_x\partial_x+\kappa_y\partial_y)\psi_{-1}+\lambda_2\psi_{-1}^*\psi_0^2, \quad (2)\\ \mathrm{i}\frac{\partial\psi_0}{\partial t}=&\Big(-\frac{1}{2}\nabla^2+V+\mathrm{i}\Omega(x\partial_y-y\partial_x)+\lambda_0\rho\\&+\lambda_2(\rho_1+\rho_{-1})\Big)\psi_0+(-\mathrm{i}\kappa_x\partial_x+\kappa_y\partial_y)\psi_1\\&+(-\mathrm{i}\kappa_x\partial_x-\kappa_y\partial_y)\psi_{-1}+2\lambda_2\psi_1\psi_{-1}\psi_0^*, \quad (3)\\ \mathrm{i}\frac{\partial\psi_{-1}}{\partial t}=&\Big(-\frac{1}{2}\nabla^2+V+\mathrm{i}\Omega(x\partial_y-y\partial_x)+\lambda_0\rho\\&+\lambda_2(\rho_0+\rho_{-1}-\rho_1)\Big)\psi_{-1}+(-\mathrm{i}\kappa_x\partial_x+\kappa_y\partial_y)\psi_0\\&+(-\mathrm{i}\kappa_x\partial_x-\kappa_y\partial_y)\psi_1+\lambda_2\psi_1^*\psi_0^2, \quad (4)\end{aligned}$$

where $\psi_j=N^{-1/2}a_{\mathrm{h}}\Psi_j$ $(j=0,\pm1)$ describes the dimensionless wave function of the condensed matter atomic distribution in each hyperfine state, and the wave function satisfies the

normalization condition $\int \mathrm{d}^2\boldsymbol{r}\psi^\dagger\psi = 1$. The dimensionless external potential of a 2D harmonic trap can be expressed as $V(\boldsymbol{r}) = (1/2)(x^2+y^2)$. Ω represents the dimensionless rotation frequency. $\rho = \rho_1+\rho_0+\rho_{-1}$ denotes the density of total particle number, where $\rho_j = |\psi_j|^2$ $(j = 1,0,-1)$. The dimensionless interaction strengths are $\lambda_0 = 4\pi N(a_0+2a_2)/3a_\mathrm{h}$ and $\lambda_2 = 4\pi N(a_2-a_0)/3a_\mathrm{h}$, respectively. We choose $a_2 = (100.4\pm0.1)a_\mathrm{B}$ for total spin channel $F_\mathrm{total} = 2$ and $a_0 = (101.8\pm0.2)a_\mathrm{B}$ for total spin channel $F_\mathrm{total} = 0$, where a_B is the Bohr radius. κ_x and κ_y are the dimensionless strengths of SU(3) SOC in the x and y directions. The characteristic length of harmonic trap is $a_\mathrm{h} = \sqrt{\hbar/m\omega}$. In the process of numerical calculation, the length, time, energy, strength of SU(3) SOC are scaled by $\sqrt{\hbar/m\omega}$, ω^{-1}, $\hbar\omega$, and $\sqrt{\hbar\omega/m}$, respectively. The ground state of the system is obtained by solving the nonlinear equations and using the standard imaginary-time propagation method,[54–56] in which the Fourier spectrum method is used for spatial discretization, and the backward and forward Euler schemes of the linear and nonlinear terms for the time discretization. The size of computational grid is 300×300, corresponding to actual calculation system being $24\times24a_\mathrm{h}^2$.

3. Results and discussion

3.1. The ground state phase without rotation

Firstly, the effect of isotropic SU(3) SOC on the ground state of the system without rotation is discussed. The particle number density and phase distributions of ground state are shown in Fig. 1. Columns 1–3 are the $m_\mathrm{F} = 1$, $m_\mathrm{F} = 0$, and $m_\mathrm{F} = -1$ component density distributions, respectively. Column 4 is the total density distribution of the three components, and columns 5–7 are the corresponding phase distributions. For the antiferromagnetic system, as shown in Figs. 1(a1) and 1(a2), the density diagrams of the system present triangular lattice distributions with spontaneous breaking of spatial translation symmetry, and the total density diagrams present circular Gaussian wave packets. The phase diagrams show the hexagonal structure formed around vortices and anti-vortices. According to the study of antiferromagnetic lattice phase by Han *et al.*, there are two different topological defects in the system, namely, double-quantum spin vortex and half-shyrmion.[37] With the increase of SU(3) SOC strength, the number of triangular lattices in the density diagrams increases with the arrangement becoming tighter. For the ferromagnetic system, as shown in Figs. 1(b1) and 1(b2), the density diagrams present circular Gaussian wave packets. Due to the dual effects of SU(3) SOC and spin-exchange interaction, the system presents a plane-wave phase. The direction of the spatial translation symmetry of the phase changes with the increase of SU(3) SOC strength.

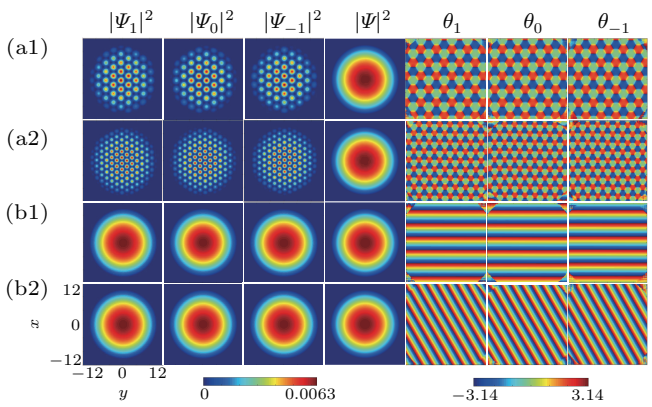


Fig. 1. Particle number densities (the first, second, third, and fourth columns) and phase distributions (the fifth, sixth and seventh columns) of the spin-1 BECs of ^{87}Rb for the different isotropic SU(3) SOC strengths. The parameters are set as follows: (a1) $\lambda_2 = 80$, $\kappa = 0.8$; (a2) $\lambda_2 = 80$, $\kappa = 1.2$; (b1) $\lambda_2 = -80$, $\kappa = 0.8$; (b2) $\lambda_2 = -80$, $\kappa = 1.2$. The rest of parameters are $\lambda_0 = 8000$, $\Omega = 0.0$, and $\omega = 2\pi\times250$ Hz.

3.2. The ground state phase with rotation

The rotating effect is considered here. Due to the rotation potential, each component of the system appears vortices. In this case, the phenomena of antiferromagnetic and ferromagnetic system are similar. We take the ferromagnetic system as an example. With fixing the rotation frequency $\Omega = 0.2$, when the SU(3) SOC strength is small, the density diagrams in Fig. 2(a) clearly show that the particle number of $m_\mathrm{F} = 0$ component is the largest, $m_\mathrm{F} = -1$ component is less, and the $m_\mathrm{F} = 1$ component is the least. With the increase of SU(3) SOC strength, the particle number of the three components gradually tends to be more evenly distributed, namely, $|\Psi_1|^2 = |\Psi_0|^2 = |\Psi_{-1}|^2 = N/3$, as shown in Fig. 2(d). Now, the three components show obvious phase separation. It shows that $m_\mathrm{F} = 1$ component is separated from $m_\mathrm{F} = 0$ component and $m_\mathrm{F} = -1$ component, respectively. The density diagrams show three vortex chains with an angle of 120° to each other along the coupling directions. The left vortex chain is arranged along the y axis, and the right two are symmetrically distributed along the y axis. There are also a few vortices in the regions between two vortex chains. Among them, each vortex actually corresponds to a half-skyrmion in the spin texture. Therefore, the vortex chain is also called the half-skyrmion chain, which will be discussed in detail below. With the increase of SU(3) SOC strength, the number of half-skyrmions on the three chains increases obviously, and the arrangement becomes increasingly tighter. This is due to the enhanced coupling between atomic spin and atomic mass center motion, and the spin flips frequently in the system, which leads to the gradual increase of the half-skyrmion number along the coupling directions. The number of half-skyrmions in the regions between two chains does not change significantly. Meanwhile, there are many phase secants in the phase diagrams. There is a discontinuous shift in the phase from $-\pi$ to π, i.e., from the blue side of the secant to the red side. The minimum point in

the density distribution diagrams corresponding to the end of the phase secant line is the vortex core. It can be clearly seen from the phase diagrams that there are three vortex chains with an angle of 120° to each other, and four obvious vortex cores in other regions. The regions formed by two vortex chains present plane wave phases, of which the phase changes from small to large in a direction perpendicular to the extension line of the third vortex chain, forming a counterclockwise winding, as shown by the arrows in Fig. 2(a).

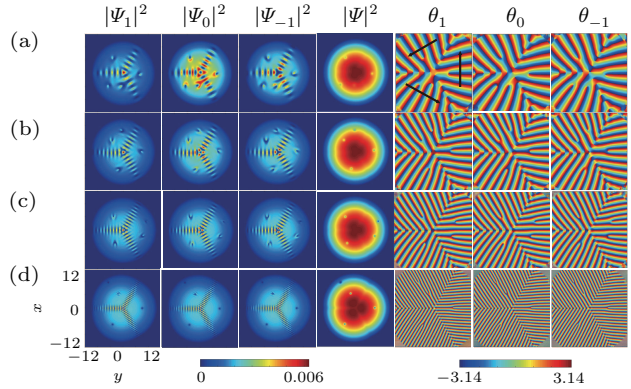


Fig. 2. Particle number densities (the first, second, third, and fourth columns) and phase distributions (the fifth, sixth and seventh columns) of the spin-1 ferromagnetic BECs of ^{87}Rb for the isotropic SU(3) SOC strengths. The parameters are set as follows: (a) $\kappa = 0.6$; (b) $\kappa = 1.0$; (c) $\kappa = 1.4$; (d) $\kappa = 2.0$. The rest of parameters are $\lambda_0 = 8000$, $\lambda_2 = -80$, $\Omega = 0.2$, and $\omega = 2\pi \times 250$ Hz.

Next, the SU(3) SOC strength is fixed, and the influence of rotation frequency on the system is considered. When the rotation frequency is small $\Omega = 0.2$, as shown in Fig. 3(a), the system presents three half-skyrmion chains, and the areas between two chains present five half-skyrmions. On the one hand, as the rotation frequency gradually increases, the number of half-skyrmions on the three chains gradually increases, and the arrangement becomes tighter. The number of half-skyrmions in the regions between two chains also gradually increases. On the other hand, it can be seen from the density diagrams that the number of particles in the system $m_F = 1$ component is the largest, followed by $m_F = 0$ and $m_F = -1$. The phenomenon becomes more obvious with the increase of the rotation frequency. Meanwhile, three half-skyrmion chains in total density diagrams become clearer, and the surface area distribution of condensate gradually increases. When the rotation frequency $\Omega = 0.8$, three half- skyrmion chains divide the condensate into a cloverleaf-like pattern.

On the whole, for the rotating BECs, the isotropic SU(3) SOC mainly regulates the number of half-skyrmions on the three chains, but has little effect on the number of half-skyrmions in the areas between two chains. The rotation frequency can not only change the number of half-skyrmions on the three chains, but also change the number of half-skyrmions in other regions.

The effects of different atomic density–density and spin-dependent interactions on the ground state are further investigated. Taking Fig. 2(b) as a reference, it can be seen from Fig. 4(a1) that when the atomic density–density interaction decreases, the number of half-skyrmions decreases. When the atomic density–density interaction increases, as shown in Fig. 4(a2), the number of half-skyrmions increases, so does the surface area distribution of the condensate. This is because the number of topological defects in the condensate is linearly related to the surface area distribution of the condensate under rotation condition, and the enhancement of atomic density–density interaction can also change the magnetic order distribution within the system, which will lead to the increase of topological defects in the condensate. As can be seen from Figs. 4(b1) and 4(b2), different spin-dependent interactions have little influence on the ground state of the system.

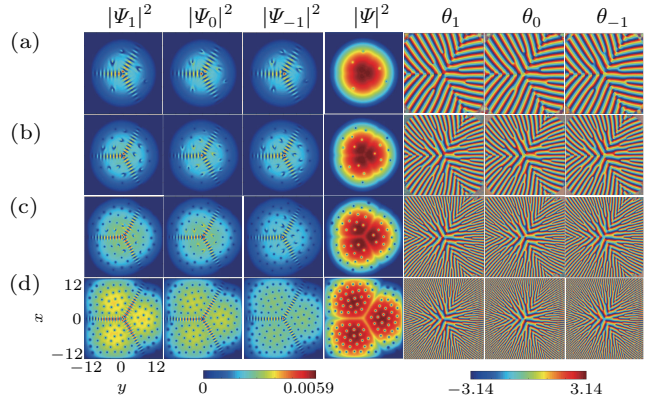


Fig. 3. Particle number densities (the first, second, third, and fourth columns) and phase distributions (the fifth, sixth and seventh columns) of the spin-1 ferromagnetic BECs of ^{87}Rb for different rotation frequencies. The parameters are set as follows: (a) $\Omega = 0.2$; (b) $\Omega = 0.4$; (c) $\Omega = 0.6$; (d) $\Omega = 0.8$. The rest of parameters are $\lambda_0 = 8000$, $\lambda_2 = -80$, $\kappa = 1.2$, and $\omega = 2\pi \times 250$ Hz.

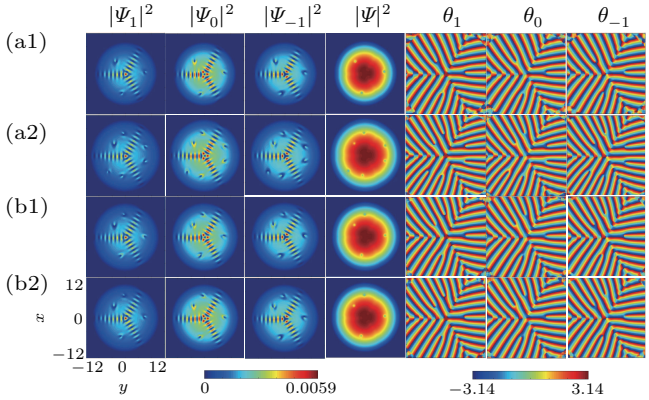


Fig. 4. Particle number densities (the first, second, third, and fourth columns) and phase distributions (the fifth, sixth and seventh columns) of the spin-1 ferromagnetic BECs of ^{87}Rb for the different atomic density–density and spin-independent interactions. The parameters are set as follows: (a1) $\lambda_0 = 6000$, $\lambda_2 = -80$; (a2) $\lambda_0 = 10000$, $\lambda_2 = -80$; (b1) $\lambda_0 = 8000$, $\lambda_2 = -60$; (b2) $\lambda_0 = 8000$, $\lambda_2 = -100$. The rest of parameters are $\Omega = 0.2$, $\kappa = 1.0$ and $\omega = 2\pi \times 250$ Hz.

In order to present more intuitively the relationships of total number of half-skyrmions on the three chains with isotropic SU(3) SOC strength (κ), rotating frequency (Ω), and atomic

density–density interaction strength (λ_0), we calculate a large number of parameters. The results are shown in Fig. 5. It can be seen that the total number of half-skyrmions on the three chains increases approximately linearly with the increase of SU(3) SOC strength and rotation frequency, but increases gradually and slowly with the increase of atomic density–density interaction, and finally the curve becomes flat. Physically, it is not difficult to analyze that as the atomic density–density interaction increases, the number of atoms increases and the gap between atoms decreases. In the case of rotation, vortices will be more difficult to generate. Thus, the SU(3) SOC and rotation effects are more significant for increasing the number of half-skyrmions on the three chains than atomic density–density interaction.

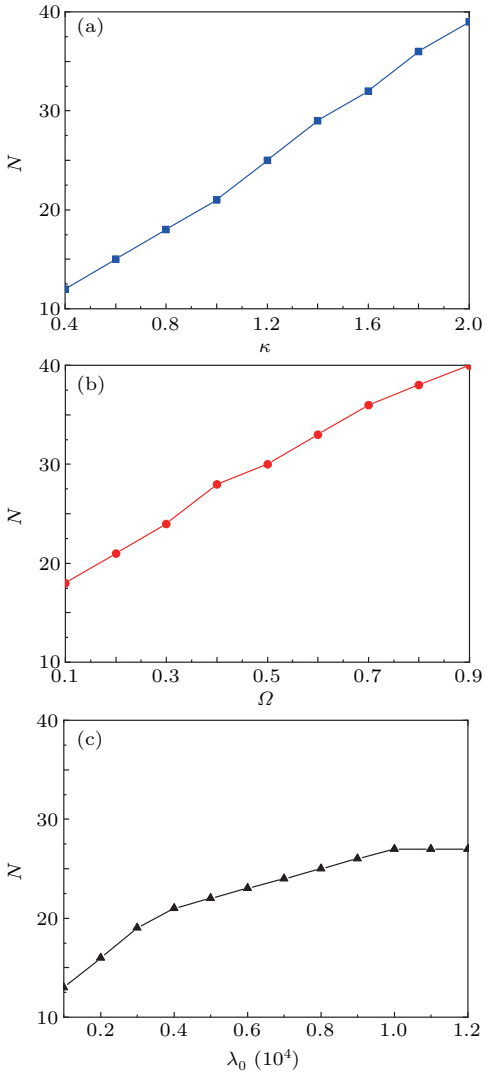


Fig. 5. Diagrams of the total number of half-skyrmions on three chains in spin-1 ferromagnetic ^{87}Rb BECs as functions of isotropic SU(3) SOC strengths (κ), rotation frequency (Ω), and density–density interaction strengths (λ_0). The parameters are set as follows: (a) $\Omega = 0.2$, $\lambda_0 = 8000$, $\lambda_2 = -80$; (b) $\kappa = 1.0$, $\lambda_0 = 8000$, $\lambda_2 = -80$; (c) $\Omega = 0.3$, $\kappa = 1.0$, $\lambda_2 = -80$. The rest of parameters is $\omega = 2\pi \times 250$ Hz.

In addition, we consider the influence of anisotropic SU(3) SOC on the ground state of the rotating system. With fixing the rotation frequency $\Omega = 0.2$ and the SU (3) SOC strength in the x direction $\kappa_x = 1.0$, when the SU (3) SOC strength in the y direction κ_y is small, as shown in Fig. 6(a), the three components of the system show phase separation obviously, and the density diagrams present three half-skyrmion chains, among which a half-skyrmion chain on the left is arranged along the y axis, and two half-skyrmion chains on the right are symmetrically distributed along the y axis. The regions between two chains also have a few half-skyrmions. Compared with Fig. 2(b), the angles between two chains are no longer 120° to each other, instead, the angle between two chains on the right is enlarged. Besides, the intersection point of the three chains is no longer at the central position, but at the left side of the central position. With the increase of κ_y, the two chains on the right gradually move to the y axis, with the angle between them decreases gradually, and the intersection point of the three half-skyrmion chains move to the right along the y axis. Finally, a half-skyrmion chain arranged tightly along the y axis is formed, with a few half-skyrmions in the upper and lower parts. Meanwhile, the ground states of the system are calculated at different κ_x with a fixed $\kappa_y = 1.0$. It is found that as the κ_x increases, the changes of the half-skyrmion chains of the system present the inverse process as shown in Fig. 6, that is, one half-skyrmion chain distributed along the y axis gradually changes to three half-skyrmion chains, and the intersection point of the three half-skyrmion chains gradually moves to the left along the y axis. It can be seen that the number and morphology of half-skyrmion chains in the system can be regulated by adjusting the anisotropic SU(3) SOC strengths in different directions.

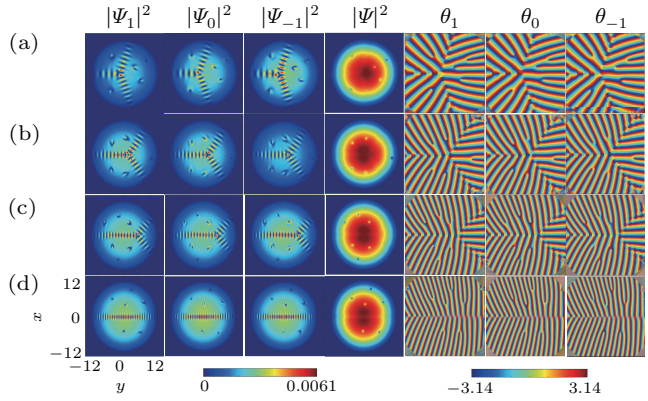


Fig. 6. Particle number densities (the first, second, third, and fourth columns) and phase distributions (the fifth, sixth and seventh columns) of the spin-1 ferromagnetic BECs of ^{87}Rb for the anisotropic SU(3) SOC strengths. The parameters are set as follows: (a) $\kappa_y = 0.6$; (b) $\kappa_y = 1.2$; (c) $\kappa_y = 1.6$; (d) $\kappa_y = 2.1$. The rest of parameters are $\kappa_x = 1.0$, $\lambda_0 = 8000$, $\lambda_2 = -80$, $\Omega = 0.2$, and $\omega = 2\pi \times 250$ Hz.

3.3. The spin textures of different ground states

Finally, we discuss the spin textures of different ground states, and define the spin vectors of components as[53]

$$F_x = [\psi_1^* \psi_0 + \psi_0^* (\psi_1 + \psi_{-1}) + \psi_{-1}^* \psi_0]/\sqrt{2}, \quad (5)$$

$$F_y = \mathrm{i}[-\psi_1^* \psi_0 + \psi_0^* (\psi_1 - \psi_{-1}) + \psi_{-1}^* \psi_0]/\sqrt{2}, \quad (6)$$

$$F_z = |\psi_1|^2 - |\psi_{-1}|^2. \tag{7}$$

The topological charge is expressed as $Q = (1/4\pi)\int\int \boldsymbol{s}\cdot[(\partial \boldsymbol{s}/\partial x)\times(\partial \boldsymbol{s}/\partial y)]\,\mathrm{d}x\mathrm{d}y$. And $\rho = (\boldsymbol{s}/4\pi)\cdot[(\partial \boldsymbol{s}/\partial x)\times(\partial \boldsymbol{s}/\partial y)]$ is the topological charge density. The spin texture in Fig. 7(a) corresponds to Fig. 1(a1). At this time, the system presents two kinds of topological defects. One is double-quantum spin vortex which has a spin current with two quanta of circulation around the unmagnetized core, as shown in the circle in Fig. 7(a). The other is the half-skyrmion with different winding combinations, as shown in the triangle or rectangle in Fig. 7(a), whose spin flips from the surrounding plane to the center or from the center to the surrounding plane, respectively. Figures 7(b) and 7(c) represent the spin textures corresponding to Figs. 1(b1) and 1(b2). Now, as the rotation frequency is zero, no spin texture corresponds to the topological defect in the ferromagnetic system. However, with the enhancement of SU(3) SOC strength, the rightward spin distribution along y axis changes from the bottom right to the top left. This is because the ferromagnetic interaction tends to make the spin be arranged in the same direction, and the increase of the coupling between the atomic spin and the motion of center mass leads to the change of the spin texture. The competition with each other results in the overall change of the spin direction. Figure 7(d) represents the spin texture corresponding to Fig. 2(b). The topological charge corresponding to each topological defect in the system is calculated as 0.5. According to Liu's research,[43] the topological charge of the vortex in the SOC rotating BEC system is calculated to be 0.5 by giving three expressions of the spin vector. Such a spin texture is called half-skyrmion. It can be clearly seen that there are three half-skyrmion chains at an angle of 120° to each other, and four half-skyrmions in the areas between two chains.

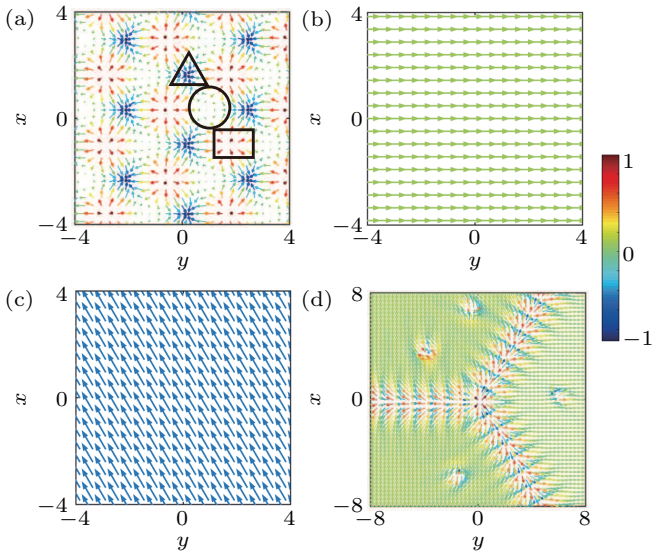


Fig. 7. The spin textures of the ground states: (a) spin texture corresponding to Fig. 1(a1); (b) spin texture corresponding to Fig. 1(b1); (c) spin texture corresponding to Fig. 1(b2); (d) spin texture corresponding to Fig. 2(b). Values of spin density are from −1 (blue) to 1 (red).

4. Conclusion

In summary, we found that in the SU(3) SOC rotating BECs system, the ferromagnetic and antiferromagnetic systems present three half-skyrmion chains at an angle of 120° to each other along the coupling directions. With the enhancement of isotropic SU(3) SOC strength, the position of the three chains remains unchanged, in which the number of half-skyrmion increases gradually. With the increase of rotation frequency and atomic density–density interaction, the number of half-skyrmions on the three chains and in the regions between two chains increases gradually. Besides, the surface area distribution of the condensate increases. However, different spin-dependent interactions have little effect on the ground state. In addition, changing the anisotropic SU(3) SOC strength in different directions can regulate the number and morphology of half-skyrmion chains. In future work, we can consider the ground state structure of rotating BECs system with SU(3) SOC and spin–orbital angular momentum coupling[57] under gradient magnetic field. We can also consider high spin system, such as spin-2 BECs,[58] and adjust different parameters, thus to greatly enrich the ground state phase diagram.

References

[1] Sadler L E, Higbie J M, Leslie S R, Vengalattore M and Stamper-Kurn D M 2006 *Nature* **7109** 312
[2] Lobo C, Sinatra A and Castin Y 2004 *Phys. Rev. Lett.* **92** 020403
[3] Ji A C, Liu W M, Song J L and Zhou F 2008 *Phys. Rev. Lett.* **101** 010402
[4] Khawaja U A and Stoof H 2001 *Nature* **411** 918
[5] Leslie L S, Hansen A, Wright K C, Deutsch B M and Bigelow N P 2009 *Phys. Rev. Lett.* **103** 250401
[6] Choi J Y, Kwon W J and Shin Y I 2012 *Phys. Rev. Lett.* **108** 035301
[7] Ray M W, Ruokokoski E, Kandel S, Möttönen M and Hall D S 2014 *Nature* **505** 657
[8] Ray M W, Ruokokoski E, Tiurev K, Möttönen M and Hall D S 2015 *Science* **348** 544
[9] Pietilä V and Möttönen M 2009 *Phys. Rev. Lett.* **103** 030401
[10] Hall D S, Ray M W, Tiurev K, Ruokokoski E, Gheorghe A H and Möttönen M 2016 *Nat. Phys.* **12** 478
[11] Xiao D, Chang M C and Niu Q 2010 *Rev. Mod. Phys* **82** 1959
[12] Qi X L and Zhang S C 2011 *Rev. Mod. Phys* **83** 1057
[13] Read N and Green D 2000 *Phys. Rev. Lett.* **61** 10267
[14] Lin Y J, García K J and Spielman I B 2011 *Nature* **471** 83
[15] Wang P J, Yu Z Q, Fu Z, Fu Z K, Miao J, Huang L H, Chai S J, Zhai H and Zhang J 2012 *Phys. Rev. Lett.* **109** 095301
[16] Cheuk L W, Sommer A T, Hadzibabic Z, Yefsah T, Zwierlein M W and Bakr W S 2012 *Phys. Rev. Lett.* **109** 095302
[17] Zhang J Y, Ji S C, Chen Z, Zhang L, Du Z D, Yan B, Pan G S, Zhao B, Deng Y J, Zhai H, Chen S and Pan J W 2012 *Phys. Rev. Lett.* **109** 115301
[18] Lin Y J, Compton R L, Jiménez-García K, Porto J V and Spielman I B 2009 *Nature* **462** 628
[19] Fu Z, Huang L, Meng Z, Wang P, Zhang L, Zhang S, Zhai H, Zhang P and Zhang J 2014 *Nat. Phys.* **10** 110
[20] Lin Y J, Compton R L, Jiménez-García K, Phillips W D, Porto J V and Spielman I B 2011 *Nat. Phys.* **7** 531
[21] Wang C, Gao C, Jian C M and Zhai H 2010 *Phys. Rev. Lett.* **105** 160403
[22] Ho T L and Zhang S 2011 *Phys. Rev. Lett.* **107** 150403
[23] Anderson B M, Juzeliūnas G, Galitski V M and Spielman I B 2012 *Phys. Rev. Lett.* **108** 235301

[24] Huang L H, Meng Z M, Wang P J, Peng P, Zhang S L, Chen L C, Li D H, Zhou Q and Zhang J 2016 *Nat. Phys.* **12** 540
[25] Meng Z M, Huang L H, Peng P, Li D H, Chen L C, Xu Y, Zhang C, Wang P and Zhang J 2016 *Phys. Rev. Lett.* **117** 235304
[26] Chen K J, Wu F and Hu J S 2020 *Phys. Rev. A* **102** 013316
[27] Ji S C, Zhang J Y, Zhang L, Du Z D, Zheng W, Deng Y J, Zhai H, Chen S and Pan J W 2014 *Nat. Phys.* **10** 314
[28] Wu Z, Zhang L, Sun W, Xu X T, Wang B Z, Ji S C, Deng Y J, Chen S, Liu X J and Pan J W 2016 *Science* **354** 83
[29] Ruseckas J, Juzeliúnas G, Öhberg P and Fleischhauer M 2005 *Phys. Rev. Lett.* **95** 010404
[30] Campbell D L, Juzeliúnas G and Spielman I B 2011 *Phys. Rev. A* **84** 025602
[31] Liu X J, Borunda M F, Liu X and Sinova J 2009 *Phys. Rev. Lett.* **102** 046402
[32] Anderson B M, Spielman I B and Juzeliúnas G 2013 *Phys. Rev. Lett.* **111** 125301
[33] Lan Z H and Öhberg P 2014 *Phys. Rev. A* **89** 023630
[34] Stanescu T D, Anderson B and Galitsk V 2008 *Phys. Rev. A* **78** 023616
[35] Galitski V and Spielman I B 2013 *Nature* **494** 49
[36] Barnett R, Boyd G R and Galitski V 2012 *Phys. Rev. Lett.* **109** 235308
[37] Han W, Zhang X F, Song S W, Saito H, Zhang W, Liu W M and Zhang S C 2016 *Phys. Rev. A* **94** 033629
[38] Grab T, Chhajlany R W, Muschik C A and Lewenstein M 2014 *Phys. Rev. B* **90** 195127
[39] Li H and Chen F L 2019 *Chin. Phys. B* **28** 070302
[40] Yue H X and Liu Y K 2020 *Commun. Theor. Phys.* **72** 025501
[41] Wang J G, Li Y Q and Dong Y F 2020 *Chin. Phys. B* **29** 100304
[42] Xu X Q and Han J H 2011 *Phys. Rev. Lett.* **107** 200401
[43] Liu C F, Fan H, Zhang Y C, Wang D S and Liu W M 2012 *Phys. Rev. A* **86** 053616
[44] Zhou X F, Zhou J and Wu C J 2011 *Phys. Rev. A* **84** 063624
[45] Sakaguchi H and Umeda K 2016 *J. Phys. Soc. Jpn.* **85** 064402
[46] Zhang X F, Gao R S, Wang X, Dong R F, Liu T and Zhang S G 2013 *Phys. Lett. A* **377** 1109
[47] Wang X, Tan R B, Du Z J, Zhao W Y, Zhang X F and Zhang S G 2014 *Chin. Phys. B* **23** 070308
[48] Wang H, Wen L H, Yang H, Shi C X and Li J H 2017 *J. Phys. B: At. Mol. Opt. Phys.* **50** 155301
[49] Radić J, Sedrakyan T A, Spielman I B and Galitski V 2011 *Phys. Rev. A* **84** 063604
[50] Fetter A L 2014 *Phys. Rev. A* **89** 023629
[51] Liu C F and Liu W M 2012 *Phys. Rev. A* **86** 033602
[52] Wang J G, Xu L L and Yang S J 2017 *Phys. Rev. A* **96** 033629
[53] Arfken G B, Weber H J and Harris F E 2000 *Mathematical Methods for Physicists* (Elsevier: Academic Press)
[54] Li J, Yu Y M, Zhuang L and Liu W M 2017 *Phys. Rev. A* **95** 043633
[55] Li J, Zhang X F and Liu W M 2018 *Ann. Phys.* **396** 87
[56] Zhang X F, Dong R F, Liu T, Liu W M and Zhang S G 2012 *Phys. Rev. A* **86** 063628
[57] Chen H R, Lin K Y, Chen P K, Chiu N C, Wang J B, Chen 1 C A, Huang P P, Yip S K, Kawaguchi Y and Lin Y J 2018 *Phys. Rev. Lett.* **121** 113204
[58] Gautam S and Adhikari S K 2015 *Phys. Rev. A* **91** 013624